IVYSPRING INTERNATIONAL PUBLISHER

Theranostics

2019; 9(26): 8312-8320. doi: 10.7150/thno.37128

Research Paper

On-demand PEGylation and dePEGylation of PLA-based nanocarriers *via* amphiphilic mPEG-*TK*-Ce6 for nanoenabled cancer chemotherapy

Yueqiang Zhu[1*], Chao Chen[1*], Ziyang Cao[2*], Song Shen[2✉], Laisheng Li[3], Dongdong Li[2], Junxia Wang[2], Xianzhu Yang[2✉]

1. School of Food and Biological Engineering, Hefei University of Technology, Hefei, Anhui, 230009, China
2. Institutes for Life Sciences, School of Medicine, South China University of Technology, Guangzhou, Guangdong 510006, China
3. Department of Laboratory Medicine, The First Affiliated Hospital of Sun Yat-sen University, Guangzhou, 510080, People's Republic of China

[*] These authors contributed equally to this work.

✉ Corresponding authors: E-mail: yangxz@scut.edu.cn (Xianzhu Yang), E-mail: shensong@scut.edu.cn (Song Shen)

Received: 2019.05.29; Accepted: 2019.10.11; Published: 2019.10.22

Abstract

Rationale: PEGylation of nanocarriers could extend blood circulation time and enhance tumor accumulation *via* the enhanced permeability and retention (EPR) effect. Unfortunately, the PEG moiety suppresses tumor cell internalization of nanocarriers, resulting in limited therapeutic efficiency (known as the PEG dilemma). Designing stimuli-responsive shell-detachable nanocarriers, which could detach the PEG corona from the nanocarriers in desired tumor tissues in response to the local environment, is an appealing approach to overcome the PEG dilemma, but nanocarrier applications are also limited by a lack of universal stimuli for PEG detachment.

Methods: In this study, we synthesized red light-responsive, amphiphilic mPEG bridged to the photosensitizer Ce6 *via* a thioketal (*TK*) bond (mPEG-*TK*-Ce6), which was then used to achieve the PEGylation of polylactide (PLA)-based nanoparticles encapsulating the Pt(IV) prodrug. The therapeutic efficacy of the prepared nanoparticles was evaluated *in vitro* and *in vivo*.

Results: We demonstrated that the amphiphilic mPEG-*TK*-Ce6 can realize the PEGylation of Pt(IV) prodrug-loaded PLA nanoparticles and consequently enhanced nanoparticle accumulation in tumor tissues. When the tumor tissues were subjected to 660 nm irradiation, reactive oxygen species (ROS) generated by Ce6 induced the rapid degradation of the adjacent *TK* bond, resulting in PEG detachment and enhanced tumor cell internalization. Therefore, mPEG-*TK*-Ce6 facilely achieved PEGylation and light-responsive dePEGylation of the nanocarrier for enhanced antitumor efficacy in nanomedicine.

Conclusion: Such red light-responsive amphiphilic mPEG-*TK*-Ce6 facilely achieved PEGylation and dePEGylation of the nanocarrier, providing a facile strategy to overcome PEG dilemma.

Key words: PEGylation, dePEGylation, photocleavable molecule, nanocarrier, cancer therapy

Introduction

Coating the surface of antitumor nanocarriers with polyethylene glycol (PEG), i.e., PEGylation, is the most widely used strategy to inhibit protein adsorption and prevent rapid elimination [1-5], consequently extending the blood circulation time, enhancing tumor accumulation *via* the enhanced permeability and retention (EPR) effect, and decreasing collateral damage to normal healthy tissues. Several PEGylated nanomedicines, including PEGylated liposomal doxorubicin (Doxil®) and the

PEG-PLA micelle form of paclitaxel (Genexol-PM®), have been approved for the treatment of malignant tumors [6-9], and many PEGylated nanodrugs have entered clinical trials. As expected, PEGylation has achieved improved tumor enrichment of nanoparticles after systemic administration; however, PEGylation also hinders the internalization of nanocarriers, resulting in limited therapeutic efficiency [10-13]. Therefore, it is highly desirable to develop a facile strategy to achieve the on-demand PEGylation and dePEGylation of nanocarriers according to the requirements.

An appealing approach for overcoming the PEG dilemma is the design of shell-detachable nanocarriers, which detach the PEG corona from nanocarriers in the tumor tissues in response to the local environment, subsequently promoting cellular uptake and enhancing antitumor efficacy [14-18]. Therefore, endogenous stimuli in the tumor microenvironment, such as acidic pH [19-21], hypoxia [22-23], and overexpression of certain enzymes [24-25], have been utilized to develop PEG-detachable nanoparticles. However, due to the heterogeneity of tumors, the pH of the extracellular environment and the dynamically varied expression of enzymes in different types of tumors in different stages or in different parts of the same tumor [26-28], the broader applicability of tumor microenvironment-responsive nanoparticles is limited. Thus, exploring alternative and generally applicable strategies for tumor-specific PEG detachment is urgently needed.

In recent years, red and near-infrared (NIR) light (650-950 nm), which are triggers for photothermal and photodynamic therapy, have received tremendous attention because of several advantages [29-33]. Light in the red and NIR regions is also considered an external stimulus and used in stimuli-responsive drug delivery systems [34-38]. Recently, it has been reported that reactive oxygen species (ROS) generated by photosensitizers under irradiation readily cleave thioketal (*TK*) bonds [39-42]. Therefore, an innovative molecule, amphiphilic mPEG bridged to the photosensitizer Ce6 *via* a *TK* bond (mPEG-*TK*-Ce6), was synthesized and used to achieve the PEGylation of polylactide (PLA)-based nanoparticles encapsulating the prodrug Pt(IV). The prepared nanocarrier is referred to as $TCNP_{Pt}$. PEGylation protects nanocarriers from rapid elimination, consequently enhancing the extravasation of nanoparticles from vessels into tumor tissues. When the tumor was subjected to 660 nm irradiation, ROS generated by Ce6 induced the rapid degradation of adjacent *TK* bonds and dePEGylation of $TCNP_{Pt}$, facilitating tumor cell internalization and improving chemotherapeutic effects (Figure 1). We systematically evaluated the effect of the on-demand PEGylation and dePEGylation of $TCNP_{Pt}$ with the assistance of red light on the cellular uptake, blood circulation, tumor accumulation, and antitumor efficacy.

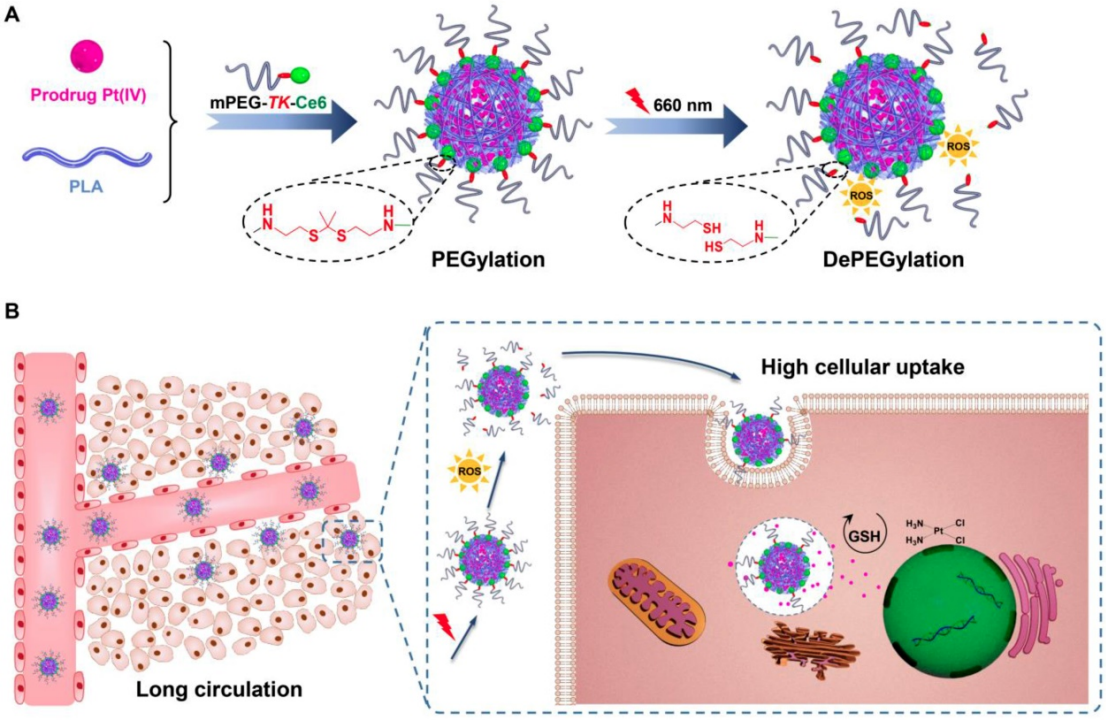

Figure 1. (A) Schematics showing the on-demand PEGylation and dePEGylation of nanocarriers *via* amphiphilic mPEG-*TK*-Ce6. (B) The PEGylation of $TCNP_{Pt}$ efficiently prolonged the circulation time. Then, the dePEGylation of $TCNP_{Pt}$ at the tumor site was achieved by cleaving the adjacent *TK* bond of mPEG-*TK*-Ce6 after irradiation to enhance cellular uptake.

Materials and Methods

Preparation and characterization of $TCNP_{Pt}$

To prepare Pt(IV) prodrug-encapsulated nanoparticles ($TCNP_{Pt}$), $mPEG_{45}$-*TK*-Ce6 (5.0 mg), PLA_{40} (5.0 mg, the synthesis described in supporting information) and Pt(IV) (2.5 mg) were dissolved in dimethyl sulfoxide (DMSO, 1.0 mL), and then added dropwise to ultrapure water (10.0 mL) for 2 h. This solution was dialyzed against ultrapure water for 24 h and filtered through a 0.45 μm filter. Similarly, fluorescein isothiocyanate (FITC)-labeled nanocarriers $^{FITC}TCNP_{Pt}$ were fabricated by the addition of FITC-labeled PLA (0.2 mg) to the preparation. The size and morphology of $TCNP_{Pt}$ were determined by light scattering (Malvern Zetasizer Nano ZS90) and transmission electron microscopy (TEM, JEOL-2010, Tokyo, Japan), respectively.

Degradation of $TCNP_{Pt}$ under 660 nm light

Aqueous $TCNP_{Pt}$ (5.0 mL, [Ce6] = 150 μg/mL) solution was irradiated (660 nm, 0.05 W/cm^2) for different amounts of time (0, 5, 10, and 20 min). Then, the samples were lyophilized for gel permeation chromatography (GPC) and ^{1}H NMR analysis. The degradation ratios of the *TK* bond were calculated according to previous reports [43].

In vitro cellular uptake of $^{FITC}TCNP_{Pt}$ with preirradiation

After receiving preirradiation (660 nm and 0.05 W/cm^2 for 5, 10 or 20 min), the $^{FITC}TCNP_{Pt}$ nanocarriers (0.1 mL, [FITC-PLA]= 2 μg/mL, [platinum]= 4.31 μg/mL) were cocultured with MDA-MB-231 cells. The cells were analyzed by flow cytometry (BD Biosciences, Franklin Lakes, NJ) at 2 and 4 h. In addition, portions of the samples were lyophilized for inductively coupled plasma mass spectrometry (ICP-MS) analysis of the intracellular platinum concentration. For confocal laser scanning microscopy (CLSM) observations, the treated cells were counterstained with Alexa Fluor568 phalloidin and 4',6-diamidino-2-phenylindole (DAPI) at 4 h and then analyzed by CLSM (LSM 710, Carl Zeiss, Inc., Jena, Germany).

In vitro antiproliferation assay

The $TCNP_{Pt}$ nanocarriers were preirradiated as described above and cocultured with MDA-MB-231 cells at different platinum concentrations (0.5, 1.0, 2.0 and 4.0 μM). After further incubation for 24 h, a 3-(4,5-dimethylthiazol-2-yl)-2,5-diphenyltetrazolium bromide (MTT) assay was performed to analyze cell viability. After the aforementioned treatment was administered at a platinum concentration of 2.0 μM, cell apoptosis was also examined by flow cytometric analysis.

In vivo and *ex vivo* distribution of $TCNP_{Pt}$

Mice bearing MDA-MB-231 xenografts were treated with $TCNP_{Pt}$ *via* intravenous (*i.v.*) injection and then imaged at predetermined time points by the Bruker Xtreme In-Vivo Fluorescence Imaging System (excitation, 650 nm). The injection dosages of platinum and Ce6 were 2.0 and 3.48 mg/kg, respectively. Moreover, after *i.v.* injection of $TCNP_{Pt}$ for 6 h, the tumor site of the $TCNP_{Pt}$ (L+) group was irradiated (660 nm and 0.05 W/cm^2 for 20 min). The main organs and tumors were collected at 24 h for fluorescent imaging and ICP-MS analyses.

Therapeutic efficacy *in vivo*

Mice bearing MDA-MB-231 xenografts were randomly divided into the following 6 groups (five mice per group): PBS, cisplatin, Pt(IV) prodrug-free TCNP plus irradiation (TCNP (L+)), $TCNP_{Pt}$ without irradiation ($TCNP_{Pt}$ (L-)), $TCNP_{Pt}$ plus irradiation ($TCNP_{Pt}$ (L+)) and TCNP (L+) + $TCNP_{Pt}$. The equivalent injection doses of platinum and Ce6 were 2.0 and 3.48 mg/kg, respectively. The tumor sites in the predetermined groups were irradiated (660 nm and 0.05 W/cm^2 for 20 min) at 6 h postinjection. For the TCNP (L+) + $TCNP_{Pt}$ group, TCNPs were injected (*i.v.*), the tumor was irradiated at 6 h postadministration, and $TCNP_{Pt}$ was then injected. On the 16th day following the first treatment, the tumor tissues were excised, weighed and imaged.

Results and discussion

Characterization of red light-responsive $TCNP_{Pt}$

To synthesize amphiphilic mPEG-*TK*-Ce6, carboxyl-terminated $mPEG_{45}$-COOH was first reacted with a *TK* linker and subsequently conjugated with Ce6 (Figure S1). A PLA homopolymer was synthesized using 10-hydroxydecanoic acid as the initiator under catalysis by $Sn(Oct)_2$ (Figure S2A). Then, the amphiphilic mPEG-*TK*-Ce6 with a critical aggregation concentration of 0.036 mg/mL (Figure S3) was utilized to achieve the PEGylation of the Pt(IV) prodrug-loaded PLA nanoparticle (denoted $TCNP_{Pt}$). The loading contents of Ce6 and platinum in $TCNP_{Pt}$ were 7.5 ± 0.59% and 4.31 ± 0.36%, respectively. Similarly, FITC-labeled $TCNP_{Pt}$ ($^{FITC}TCNP_{Pt}$) was prepared to track the nanocarrier (Figure S2C).

According to our design, 660 nm irradiation induced the production of ROS by the conjugated Ce6 (Figure S4), causing the cleavage of adjacent *TK* bonds and rapid dePEGylation. To demonstrate this, $TCNP_{Pt}$

was irradiated by light (660 nm and 0.05 W/cm² for 5, 10 or 20 min), and the $TCNP_{Pt}$ nanoparticles were then collected for GPC analysis. As shown in Figure 2A, the peak gradually increased at 29.2 min (Ce6) as the irradiation time increased. In addition, the $TCNP_{Pt}$ nanoparticles were lyophilized and analyzed by ^1H NMR after irradiation. As the preirradiation time increased, the amount of CH_3 from the *TK* bond of mPEG-TK-Ce6 (with a peak at 1.58 ppm) gradually decreased (Figure S5), while the peak at 2.12 ppm indicated that the amount CH_3 from acetone (the product of *TK* bond rupture) increased. Based on these ^1H NMR spectra, the degradation ratio of the *TK* bond was calculated, as shown in Figure 2B, and found to exhibit time dependence. Approximately 39.6% of the *TK* bond of mPEG-*TK*-Ce6 was cleaved after receiving 0.05 W/cm² irradiation for 30 min. These results indicated that a 660 nm laser efficiently caused PEG detachment under light irradiation.

The size, morphology, zeta potential and stability of $TCNP_{Pt}$ with or without 660 nm light irradiation were also determined. $TCNP_{Pt}$ nanoparticles were irradiated for different amounts of time (0, 5, 10, and 20 min at 0.05 W/cm²), and the nanoparticles that were not irradiated were used as a control. PEG detachment did not significantly affect the size, morphology and stability of $TCNP_{Pt}$. The $TCNP_{Pt}$ nanoparticles were approximately 120 nm in diameter (Figure 2C) and had a spherical morphology (Figure 2D). The size (Figure 2C) and zeta potentials (Figure S6) of $TCNP_{Pt}$ exhibited slightly decrease after light irradiation. And, preirradiation also caused a slight increase in the $TCNP_{Pt}$ size in 10% FBS within 6 days (Figure 2E), which could be attributed to the enhanced protein adsorption after dePEGylation. The dilution stability of $TCNP_{Pt}$ were performed with the different dilution in PBS, which showed that $TCNP_{Pt}$ maintain a stable form (Figure S7). In addition, compared with the nonirradiated condition, light-induced PEG detachment did not obviously affect the release rate of the Pt(IV) prodrug from $TCNP_{Pt}$ (Figure 2F).

Red light-induced dePEGylation enhances the cellular uptake of $TCNP_{Pt}$

The PEGylation of nanocarriers minimizes their elimination *in vivo*, and the disadvantage of PEGylation is the hindrance to cellular uptake. We proposed that red light-induced dePEGylation could overcome these limitations. To investigate this hypothesis, the cellular uptake of preirradiated $^{FITC}TCNP_{Pt}$ was examined using qualitative and quantitative methods. First, $^{FITC}TCNP_{Pt}$ was irradiated and then cocultured with MDA-MB-231 cells for 2 and 4 h (the dose of platinum was 4.31 μg/mL). Then, intracellular FITC fluorescence was analyzed by flow cytometry. As shown in Figure 3A and 3B, preirradiation of $^{FITC}TCNP_{Pt}$ obviously elevated the intracellular fluorescence signal at 2 and 4 h, and showed that preirradiation had a time-dependent effect on cellular uptake. The enhanced tumor cell uptake of the preirradiated nanoparticles was further corroborated by CLSM. Clearly, the most intracellular green fluorescence was observed when the cells were treated with $^{FITC}TCNP_{Pt}$ plus 20 min of preirradiation (Figure 3C). Furthermore, we also determined the

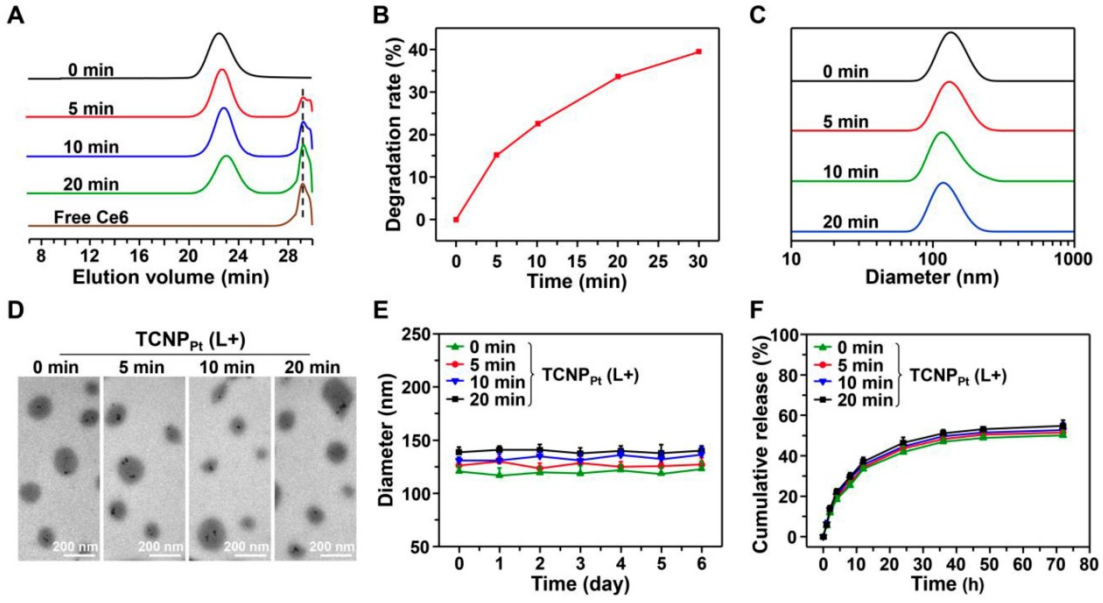

Figure 2. Characterization of red light-responsive $TCNP_{Pt}$. (A) GPC of mPEG-*TK*-Ce6 after irradiation with a 660 nm laser for different amounts of time (0.05 W/cm²). (B) The degradation of mPEG-TK-Ce6 with respect to irradiation for different amounts of time. The size (C), TEM images (D), and stability (E) of $TCNP_{Pt}$ after irradiation for different amounts of time. (F) The platinum release curve of $TCNP_{Pt}$ after 660 nm light irradiation for different amounts of time.

intracellular platinum content *via* ICP-MS. At both timepoints, preirradiation significantly elevated the intracellular platinum concentration (Figure 3D). For instance, the amount of intracellular platinum in cells treated with $^{FITC}TCNP_{Pt}$ plus 20 min of preirradiation was 1.96-fold greater than that in cells treated with $^{FITC}TCNP_{Pt}$ without preirradiation after 4 h of incubation. Thus, these results demonstrated that light-induced dePEGylation led to enhanced cellular uptake of $TCNP_{Pt}$.

Red light-induced dePEGylation significantly enhances the antiproliferative activity

We demonstrated that light-induced dePEGylation increased the amount of intracellular platinum. To further investigate the advantage of red light-responsive nanocarriers in cancer therapy, their antiproliferative activity against tumor cells was examined. $TCNP_{Pt}$ was preirradiated for different periods, and then various amounts of $TCNP_{Pt}$ were used to treat the tumor cells for the MTT assay. Figure 4A showed that tumor cell proliferation was most significantly inhibited by $TCNP_{Pt}$ plus 20 min of preirradiation at platinum concentrations of 2.0 μM or 4.0 μM. Noted that the blank nanoparticle TCNP did not exhibit obvious toxicity (Figure S8). Furthermore, after receiving these treatments, the cells were stained with annexin V-FITC and propidium iodide (PI) for the analysis of cell apoptosis. At the platinum concentrations shown in Figure 4B and 4C, $TCNP_{Pt}$ without irradiation had a negligible effect on the survival of tumor cells; however, preirradiation for 5 and 10 min induced 17.7% and 21.7% cell apoptosis, respectively. Preirradiation of $TCNP_{Pt}$ for 20 min significantly increased the percentage of apoptotic cells (30.9%). Collectively, these anticancer results verified that the red light-induced dePEGylation effect markedly increased the antiproliferative activity of the tumor cells.

Red light-induced dePEGylation improved tumor accumulation

Encouraged by the superior *in vitro* antiproliferation efficacy, animal experiments were performed to investigate the potential advantage of PEGylation during blood circulation and subsequent dePEGylation at the tumor site of $TCNP_{Pt}$ with the assistance of light. Before evaluating the antitumor efficacy, the pharmacokinetics and biodistribution of $TCNP_{Pt}$ were examined. ICR mice were injected (*i.v.*) with $TCNP_{Pt}$ and cisplatin at an identical platinum dose of 2.0 mg/kg, and the concentration of platinum in plasma over time was analyzed (Figure 5A), and the pharmacokinetic parameters were calculated in Table S1. Clearly, free cisplatin was rapidly eliminated in the blood circulation, while the circulation of $TCNP_{Pt}$ was significantly prolonged due to PEGylation.

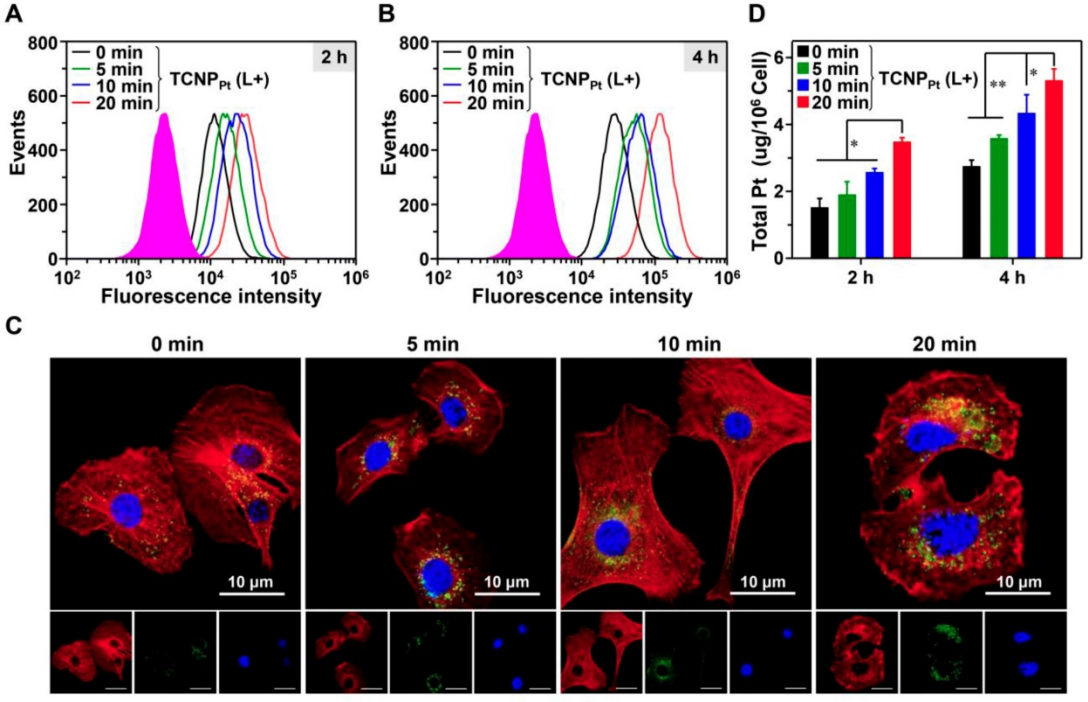

Figure 3. Red light-induced dePEGylation enhances the cellular uptake of $TCNP_{Pt}$. The cellular uptake of preirradiated $^{FITC}TCNP_{Pt}$ (0, 5, 10, and 20 min) analyzed using flow cytometry after 2 h (A) and 4 h (B) of incubation. CLSM images (C) and ICP-MS analysis (D) of cells after receiving these treatments. The green fluorescence represented the $^{FITC}TCNP_{Pt}$ singal. Cell nuclei and the cytoskeleton were stained with DAPI (Blue) and Alexa Fluor568 phalloidin (Red), respectively. The scale bar is 10 μm.

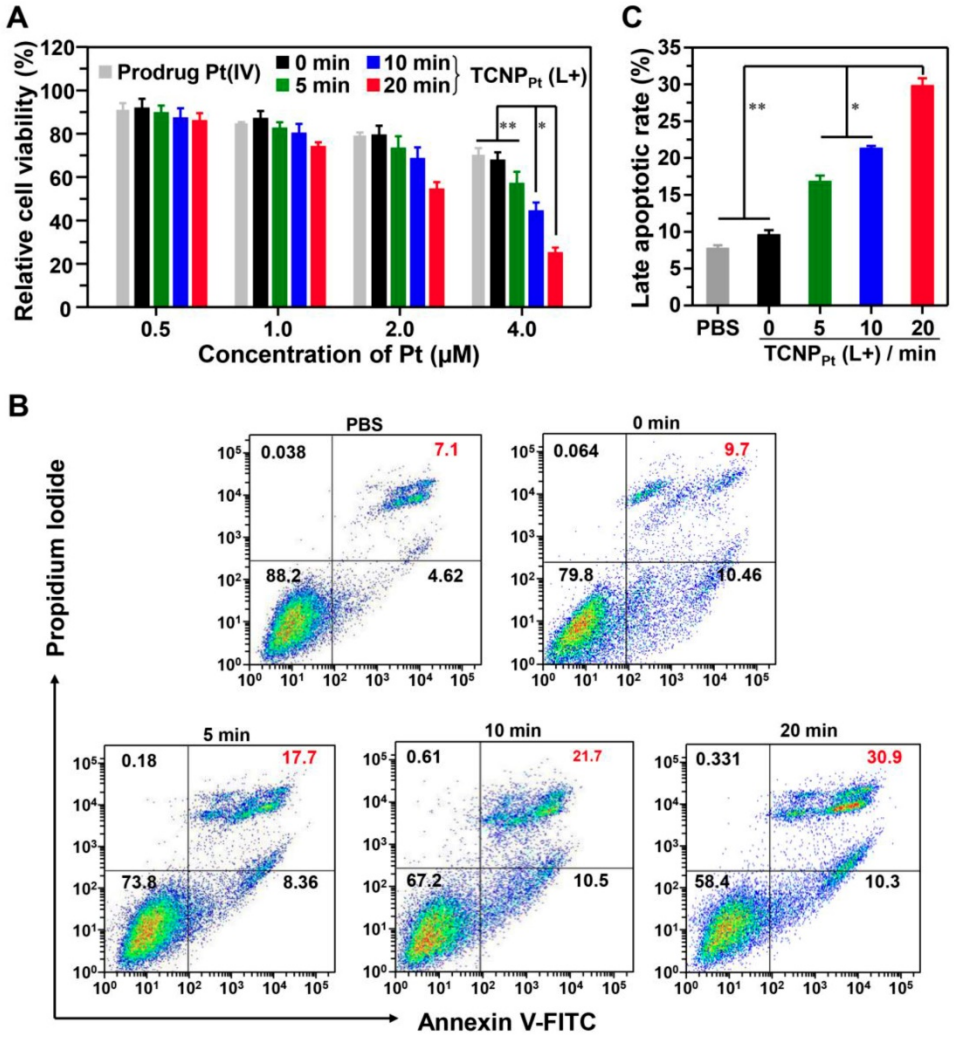

Figure 4. Red light-induced dePEGylation significantly enhances the antiproliferative activity. (A) Cell viability of preirradiated TCNP$_{Pt}$ (0, 5, 10, and 20 min) at different concentrations of TCNP$_{Pt}$. (B) Cell apoptosis induced by preirradiated TCNP$_{Pt}$ (0, 5, 10, and 20 min) at an identical platinum concentration of 2.0 μM. (C) The percentage of late apoptotic cells induced by different treatments according to flow cytometric analysis (Figure 4C).

Because TCNP$_{Pt}$ with prolonged blood circulation was readily extravasated from vessels into the tumor tissues *via* the EPR effect, the biodistribution of TCNP$_{Pt}$ was evaluated in the mice bearing MDA-MB-231 xenografts. As shown in Figure 5B, an obvious fluorescence signal was observed at the tumor sites at 1 h postinjection, and the intensity of the signal was strong until 24 h postinjection. To further verify whether the dePEGylation of TCNP$_{Pt}$ induced by red light enhances TCNP$_{Pt}$ tumor cell uptake and improves the subsequent accumulation in the tumor tissue, tumor-bearing mice were administered TCNP$_{Pt}$, and portions of the mice tumor tissues were irradiated at 6 h postinjection. The main organs were collected and observed at 24 h postinjection. As shown in Figure 5C and Figure S9, the fluorescence signal observed in the tumors in the TCNP$_{Pt}$ (L+) group was greater than that in the TCNP$_{Pt}$(L-) group, but the signal intensity of the organs in both groups was similar, indicating that the dePEGylation induced by red light enhances the internalization of the nanoparticles by the tumor cells. In addition, the platinum content at 24 h after administration was examined using ICP-MS, as shown in Figure 5D. The platinum content in the tumor tissue in the TCNP$_{Pt}$ (L+) group was 1.64-fold greater than that in the TCNP$_{Pt}$ (L-) group. Therefore, the on-demand PEGylation and dePEGylation of TCNP$_{Pt}$ assisted by light not only enhances drug accumulation in tumor tissues but also potentially reduces nonspecific cellular uptake and avoids cytotoxicity.

The on-demand PEGylation and dePEGylation of TCNP$_{Pt}$ assisted by light significantly improves the anticancer efficacy

The abovementioned results clearly showed the advantage of on-demand PEGylation and dePEGylation of TCNP$_{Pt}$ assisted by light. It is rational to speculate that tumor site-specific light irradiation

significantly increases the anticancer efficacy of $TCNP_{Pt}$. Therefore, mice bearing MDA-MB-231 xenografts were randomly divided into the following 6 groups (n = 5): PBS, cisplatin, platinum-free TCNP plus irradiation (TCNP (L+)), $TCNP_{Pt}$ without irradiation ($TCNP_{Pt}$ (L-)), $TCNP_{Pt}$ plus irradiation ($TCNP_{Pt}$ (L+)) and TCNP (L+) plus $TCNP_{Pt}$ (L-). The mice that were irradiated received the irradiation treatment at 6 h postinjection. As shown in Figure 6A, the cisplatin and $TCNP_{Pt}$ (L-) treatments only slightly inhibited tumor growth. In addition, the TCNP (L+) treatment exhibited moderate anticancer efficacy, which could be due to the photodynamic effect of the conjugated Ce6. Furthermore, the tumor-suppressive effect of $TCNP_{Pt}$ with light irradiation was much better than the combination of TCNP (L+) and $TCNP_{Pt}$ (L-), verifying that red light-induced PEG detachment significantly enhances the anticancer efficacy of $TCNP_{Pt}$. Notably, no obvious body weight loss was observed (Figure S10). In addition, the tumor images (Figure 6B) and tumor weights (Figure 6C) showed that the $TCNP_{Pt}$ (L+) group had the best anticancer efficiency.

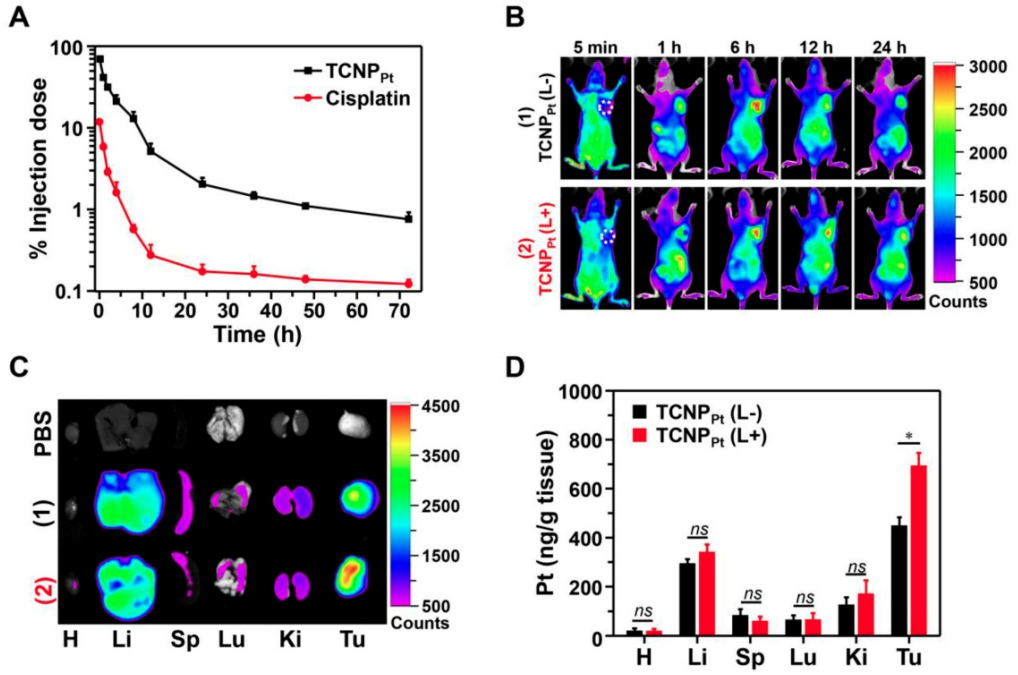

Figure 5. Red light-induced dePEGylation improved tumor accumulation. (A) The platinum concentration over time for free cisplatin and $TCNP_{Pt}$. (B) The distribution of $TCNP_{Pt}$ in MDA-MB-231 tumor-bearing mice. (C) *Ex vivo* images of the main organs at 24 h. (D) ICP-MS analysis of the platinum content in the major organs. In Figure 5B-D, $TCNP_{Pt}$ (L+) indicates that the tumor site was irradiated at 6 h.

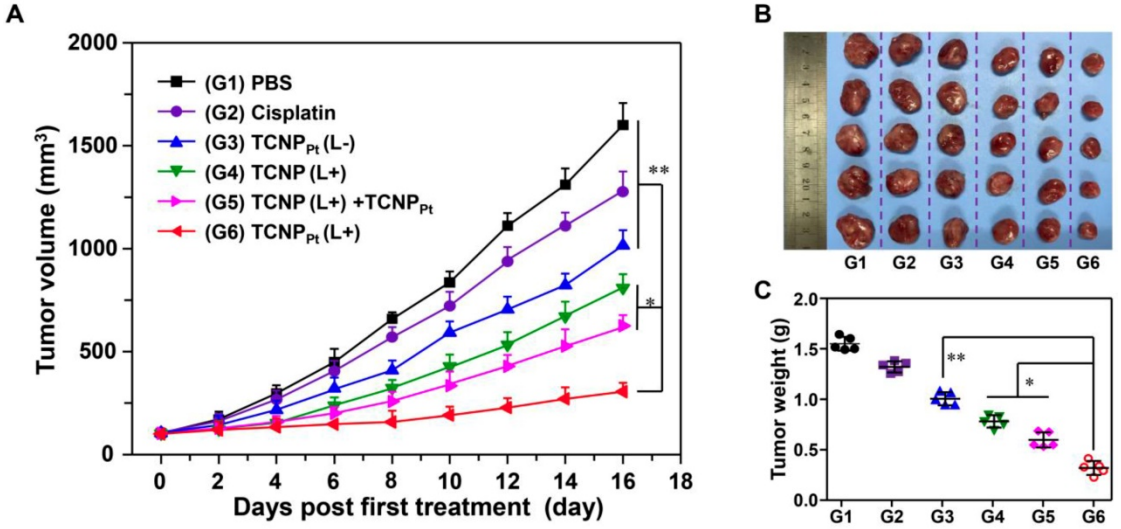

Figure 6. The on-demand PEGylation and dePEGylation of $TCNP_{Pt}$ assisted by light significantly improves the anticancer efficacy. (A) Tumor growth curves after receiving different treatments. The mice were divided into the following six groups: PBS, cisplatin, Pt(IV) prodrug-free TCNP plus irradiation (TCNP (L+)), $TCNP_{Pt}$ without irradiation ($TCNP_{Pt}$ (L-)), $TCNP_{Pt}$ plus irradiation ($TCNP_{Pt}$ (L+)) and TCNP (L+) plus $TCNP_{Pt}$ (L-). Tumor images (B) and weights (C) of the various groups on the 16th day.

Conclusion

We successfully synthesized red light-responsive, amphiphilic mPEG-*TK*-Ce6 for the on-demand PEGylation and dePEGylation of the $TCNP_{Pt}$ nanocarrier. The PEGylation of $TCNP_{Pt}$ efficiently prolonged its blood circulation after systemic administration. When a 660 nm laser was used to irradiate the tumor site, ROS generated by Ce6 in mPEG-*TK*-Ce6 cleaved the adjacent *TK* bond to cause the dePEGylation of $TCNP_{Pt}$, significantly enhancing tumor cellular uptake and the subsequent anticancer effect. Importantly, compared with other stimuli-responsive nanocarriers, red light-responsive $TCNP_{Pt}$ is more extensive and practical, and this study provides a facile strategy to achieve the on-demand PEGylation and dePEGylation of nanocarriers.

Supplementary Material

Supplementary materials and methods, figures, and table. http://www.thno.org/v09p8312s1.pdf

Acknowledgements

This work was supported by National Natural Science Foundation of China (51822302, 51773067, 81602691), the Program for Guangdong Introducing Innovative and Entrepreneurial Teams (2017ZT07S054), the Natural Science Foundation for Distinguished Young Scholars of Guangdong Province (2017B030306002), and the Fundamental Research Funds for the Central Universities.

Competing Interests

The authors have declared that no competing interest exists.

References

1. Butcher NJ, Mortimer GM, Minchin RF. Unravelling the stealth effect. Nat Nanotechnol. 2016; 11: 310-311.
2. Hu Y, Zhao ZM, Harmon T, Pentel PR, Ehrich M, Zhang CM. Paradox of PEGylation in fabricating hybrid nanoparticle-based nicotine vaccines. Biomaterials. 2018; 182: 72-81.
3. Kolate A, Baradia D, Patil S, Vhora I, Kore G, Misra A. PEG - A versatile conjugating ligand for drugs and drug delivery systems. J Control Release. 2014; 192: 67-81.
4. Pasut G, Veronese FM. State of the Art in PEGylation: The great versatility achieved after forty years of research. J Control Release. 2012; 161: 461-472.
5. Han XX, Jing XX, Yang DY, Lin H, Wang ZG, Ran HT, et al. Therapeutic mesopore construction on 2D Nb2C MXenes for targeted and enhanced chemo-photothermal cancer therapy in NIR-II biowindow. Theranostics. 2018; 8: 4491-4508.
6. Russell LM, Hultz M, Searson PC. Leakage kinetics of the liposomal chemotherapeutic agent doxil: the role of dissolution, protonation, and passive transport, and implications for mechanism of action. J Control Release. 2018; 269: 171-176.
7. Alibolandi M, Abnous K, Mohammadi M, Hadizadeh F, Sadeghi F, Taghavi S, et al. Extensive preclinical investigation of polymersomal formulation of doxorubicin versus doxil-mimic formulation. J Control Release. 2017; 264: 228-236.
8. Hu QY, Gao XL, Gu GZ, Rang T, Tu YF, Liu ZY, et al. Glioma therapy using tumor homing and penetrating peptide-functionalized PEG-PLA nanoparticles loaded with paclitaxel. Biomaterials. 2013; 34: 5640-5650.
9. Ruan G, Feng SS. Preparation and characterization of poly(lactic acid)-poly(ethylene glycol)-poly(lactic acid) (PLA-PEG-PLA) microspheres for controlled release of paclitaxel. Biomaterials. 2003; 24: 5037-5044.
10. Chen J, Ding J, Wang Y, Cheng J, Ji S, Zhuang X, et al. Sequentially responsive shell-stacked nanoparticles for deep penetration into solid tumors. Adv Mater. 2017; 29: 1701170.
11. Chen YZ, Zhang M, Jin HY, Tang YS, Wang HY, Xu Q, et al. Intein-mediated site-specific synthesis of tumor-targeting protein delivery system: turning PEG dilemma into prodrug-like feature. Biomaterials. 2017; 116: 57-68.
12. Wang S, Huang P, Chen XY. Stimuli-responsive programmed specific targeting in nanomedicine. ACS Nano. 2016; 10: 2991-2994.
13. Shiraishi K, Kawano K, Maitani Y, Aoshi T, Ishii KJ, Sanada Y, et al. Exploring the relationship between anti-PEG IgM behaviors and PEGylated nanoparticles and its significance for accelerated blood clearance. J Control Release. 2016; 234: 59-67.
14. Wei JP, Li JC, Sun D, Li Q, Ma JY, Chen XL, et al. A novel theranostic nanoplatform based on Pd@Pt-PEG-Ce6 for enhanced photodynamic therapy by modulating tumor hypoxia microenvironment. Adv Funct Mater. 2018; 28: 1706310.
15. Fan M, Zeng Y, Ruan H, Zhang Z, Gong T, Sun X. Ternary nanoparticles with a sheddable shell efficiently deliver microRNA-34a against CD44-positive melanoma. Mol Pharm. 2017; 14: 3152-3163.
16. Guan X, Guo Z, Wang T, Lin L, Chen J, Tian H, et al. A pH-responsive detachable PEG shielding strategy for gene delivery system in cancer therapy. Biomacromolecules. 2017; 18: 1342-1349.
17. Guan X, Guo Z, Lin L, Chen J, Tian H, Chen X. Ultrasensitive pH triggered charge/size dual-rebound gene delivery system. Nano Lett. 2016; 16: 16823-6831.
18. Zhu X, Tao W, Liu D, Wu J, Guo ZL, Ji XY, et al. Surface de-PEGylation controls nanoparticle-mediated siRNA delivery *in vitro* and *in vivo*. Theranostics. 2017; 7: 1990-2002.
19. Chen XH, Chen ZW, Hu BH, Cai PQ, Wang S, Xiao SZ, et al. Synergistic lysosomal activatable polymeric nanoprobe encapsulating pH sensitive imidazole derivative for tumor diagnosis. Small. 2018; 14: 1703164.
20. Wang HR, Zhu WW, Liu JJ, Dong ZL, Liu Z. pH-responsive nanoscale covalent organic polymers as a biodegradable drug carrier for combined photodynamic chemotherapy of Cancer. ACS Appl Mater Interfaces. 2018; 10: 14475-14482.
21. Sun X, Du RH, Zhang L, Zhang GL, Zheng XJ, Qian JC, et al. A pH-responsive yolk-like nanoplatform for tumor targeted dual-mode magnetic resonance imaging and chemotherapy. ACS Nano. 2017; 11: 7049-7059.
22. Xiang HJ, Lin H, Yu LD, Chen Y. Hypoxia-irrelevant photonic thermodynamic cancer nanomedicine. ACS Nano. 2019; 13: 2223-2235.
23. Huang XL, Zhuang J, Chung SW, Huang BW, Halpert G, Negron K, et al. Hypoxia-tropic protein nanocages for modulation of tumor- and chemotherapy-associated hypoxia. ACS Nano. 2019; 13: 236-247.
24. Son J, Kalafatovic D, Kumar M, Yoo B, Cornejo MA, Contel M, et al. Customizing morphology, size, and response kinetics of matrix metalloproteinase-responsive nanostructures by systematic peptide design. ACS Nano. 2019; 13: 1555-1562.
25. Wang ZH, Wang YH, Jia XQ, Han QJ, Qian YX, Li Q, et al. MMP-2-controlled transforming micelles for heterogeneic targeting and programmable cancer therapy. Theranostics. 2019; 9: 1728-1740.
26. Somasundaram R, Zhang G, Fukunaga-Kalabis M, Perego M, Krepler C, Xu XW, et al. Tumor-associated B-cells induce tumor heterogeneity and therapy resistance. Nat Commun. 2017; 8: 607.
27. Kleppe M, Levine RL. Tumor heterogeneity confounds and illuminates: assessing the implications. Nat Med. 2014; 20: 342-344.
28. Yang Q, Parker CL, McCallen JD, Lai SK. Addressing challenges of heterogeneous tumor treatment through bispecific protein-mediated pretargeted drug delivery. J Control Release. 2015; 220: 715-726.
29. Zheng B, Wang HJ, Pan HZ, Liang C, Ji WY, Zhao L, et al. Near-infrared light triggered upconversion optogenetic nanosystem for cancer therapy. ACS Nano. 2017; 11: 11898-11907.
30. Sang YH, Zhao ZH, Zhao MW, Hao P, Leng YH, Liu H. From UV to near-infrared, WS_2 nanosheet: a novel photocatalyst for full solar light spectrum photodegradation. Adv Mater. 2015; 27: 363-369.
31. Tsuji Y, Yamamoto K, Yamauchi K, Sakai K. Near-infrared light-driven hydrogen evolution from water using a polypyridyl triruthenium photosensitizer. Angew Chem Int Ed Engl. 2018; 57: 208-212.
32. Gobin AM, Lee MH, Halas NJ, James WD, Drezek RA, West JL. Near-infrared resonant nanoshells for combined optical imaging and photothermal cancer therapy. Nano Lett. 2007; 7: 1929-1934.
33. Ke HT, Wang JR, Tong S, Jin YS, Wang SM, Qu EZ, et al. Gold nanoshelled liquid perfluorocarbon magnetic nanocapsules: a nanotheranostic platform for bimodal ultrasound/magnetic resonance imaging guided photothermal tumor ablation. Theranostics. 2014; 4: 12-23.
34. Sun Q, You Q, Pang XJ, Tan XX, Wang JP, Liu L, et al. A photoresponsive and rod-shape nanocarrier: single wavelength of light triggered photothermal and photodynamic therapy based on AuNRs-capped & Ce6-doped mesoporous silica nanorods. Biomaterials. 2017; 122: 188-200.
35. Hu X, Tian HL, Jiang W, Song AX, Li ZH, Luan YX. Rational design of IR820-and Ce6-based versatile micelle for single NIR laser-induced imaging and dual-modal phototherapy. Small. 2018; 14: 1802994.
36. Sheng DL, Liu TZ, Deng LM, Zhang L, Li XL, Xu J, et al. Perfluorooctyl bromide & indocyanine green co-loaded nanoliposomes for enhanced multimodal imaging-guided phototherapy. Biomaterials. 2018; 165: 1-13.

37. Wang YY, Deng YB, Luo HH, Zhu AJ, Ke HT, Yang H, et al. Light-responsive nanoparticles for highly efficient cytoplasmic delivery of anticancer agents. ACS Nano. 2017; 11: 12134-12144.
38. Saravanakumar G, Park H, Kim J, Park D, Pramanick S, Kim DH, et al. Miktoarm amphiphilic block copolymer with singlet oxygen-labile stereospecific β-aminoacrylate junction: synthesis, self-assembly, and photodynamically triggered drug release. Biomacromolecules. 2018; 19: 2202-2213.
39. Wang M, Zhai Y, Ye H, Lv Q, Sun B, Luo C. et al. High co-loading capacity and stimuli-responsive release based on cascade reaction of self-destructive polymer for improved chemo-photodynamic therapy. ACS Nano. 2019; 13: 7010-7023.
40. Liu R, Yu M, Yang X, Umeshappa CS, Hu C, Yu W, et al. Linear chimeric triblock molecules self-assembled micelles with controllably transformable property to enhance tumor retention for chemo-photodynamic therapy of breast cancer. Adv Fun Mater. 2019; 29: 1808462.
41. Yuan YY, Liu J, Liu B. Conjugated-polyelectrolyte-based polyprodrug: targeted and image-guided photodynamic and chemotherapy with on-demand drug release upon irradiation with a single light source. Angew Chem Int Ed Engl. 2014; 53: 7163-7168.
42. Xu L, Yang Y, Zhao M, Gao W, Zhang H, Li S, et al. A reactive oxygen species–responsive prodrug micelle with efficient cellular uptake and excellent bioavailability. J Mater Chem B. 2018; 6: 1076-1084.
43. Yue C, Zhang C, Alfranca G, Yang Y, Jiang X, Yang Y, et al. Near-infrared light triggered ROS-activated theranostic platform based on Ce6-CPT-UCNPs for simultaneous fluorescence imaging and chemo-photodynamic combined therapy. Theranostics. 2016; 6:456-469.